XMM-Newton CCF Release Note

XMM-CCF-REL-332

Change in sign of the BORESIGHT psi angle

Richard Saxton

22 Jan 2016

1 CCF components

Name of CCF	VALDATE	EVALDATE	Blocks changed	XSCS flag
XMM_BORESIGHT_0026.CCF	2000-01-01		BORESIGHT	NO

2 Changes

It has been found that due to a long-standing error in a formula within the task *attcalc*, the Euler ψ angle contained within the boresight CCF has the wrong sign. In most cases the two errors cancel out and the astrometry is correctly reconstructed within the SAS. Some tasks use the incorrect boresight numbers directly, however, which results in a wrong conversion between celestial and detector coordinate systems.

With this release of the CCF, the sign of the Euler ψ angle has been inverted for the three EPIC cameras. In parallel, tasks within SAS v15, including *attcalc*, have been modified to make them compatible with the new values. Note that the OM and RGS boresight angles, were not calculated using *attcalc* and already have the correct sign in the CCF. These instruments are therefore unaffected by the change. The final Euler angle values are given in table 1, where the only change from the previous CCF is to the sign of ψ.

3 Scientific Impact of this Update

Table 1 shoes that $|\psi|$ is very small for MOS-1 but larger for the MOS-2 and EPIC-pn cameras. These translate into an error in the rotation angle of the camera which is negligible for MOS-1 but of the order of 0.3 degrees for MOS-2 and 0.2 degrees for EPIC-pn. This leads to a difference of upto ~ 9 and ~ 6 arcseconds for MOS-2 and EPIC-pn at the edge of the field of view.

Table 1: Boresight misalignment angles for the EPIC cameras

Instrument	Phi (radians)	Theta (radians)	Psi (radians)
EMOS1	3.141957521072	-2.810692725679E-04	-6.183784653418E-06
EMOS2	3.141679946362	-1.584079506320E-04	+5.097243340433E-03
EPN	3.141859308170	-5.668335763775E-04	-3.768162700000E-03

3.1 Source detection and the serendipitous source catalogue

The error in the Euler ψ angle has been compensated for by the SAS taks, in SAS versions up to and including 14. This means that the event files produced by the SAS have contained the correct detector and sky coordinates and the correct WCS header keywords. The source lists produced by the detection chain, principally the tasks, *eboxdetect, emldetect, eexpmap, attcalc*, have the correct celestial position and exposure time. Nevertheless, the RAWX, RAWY pixel values contained in the *emldetect* source lists have been calculated with an incorrect conversion. These are stored as integer numbers and differ from the true values by 0, 1 or 2 pixels in the X and/or Y axes for the EPIC-pn detector and upto 9 pixels for MOS-2. The offsets increase with increasing off-axis angle. This error will be corrected by this release.

3.2 Effective area calculation

The effective area of the telescope and detector system is calculated by the task *arfgen*. This task does not compensate for the previous ψ angle error and so the conversion between sky coordinates and detector position contains an error which becomes important at the edge of the field of view. The effect on the vignetting and encircled energy correction is negligible. However, it does affect the treatment of chip gaps, bad columns and bad pixels. When *arfgen* calculates the effect of a chip gap on the effective area of a point source, it convolves the missing CCD area with the point spread function. In extreme cases, e.g. when a source is located towards the edge of the field of view, with an extraction region bisected by a chip gap or bad column, the resulting effective area can be drastically affected by the mis-calculation of the region location on the detector.

In Fig. 1 we show the difference between the positioning of the source region on the detector with the old and new boresight CCFs, for a source near the edge of the field-of-view, which is strongly affected by a chip gap. In this case, the effective area at 1 keV calculated by *arfgen*, changes from 119 to 69 cm^2 when changing from XMM_BORESIGHT_0024.CCF to XMM_BORESIGHT_0026.CCF. Note that this is an extreme case and the majority of sources will not experience a significant change in effective area with the new CCF.

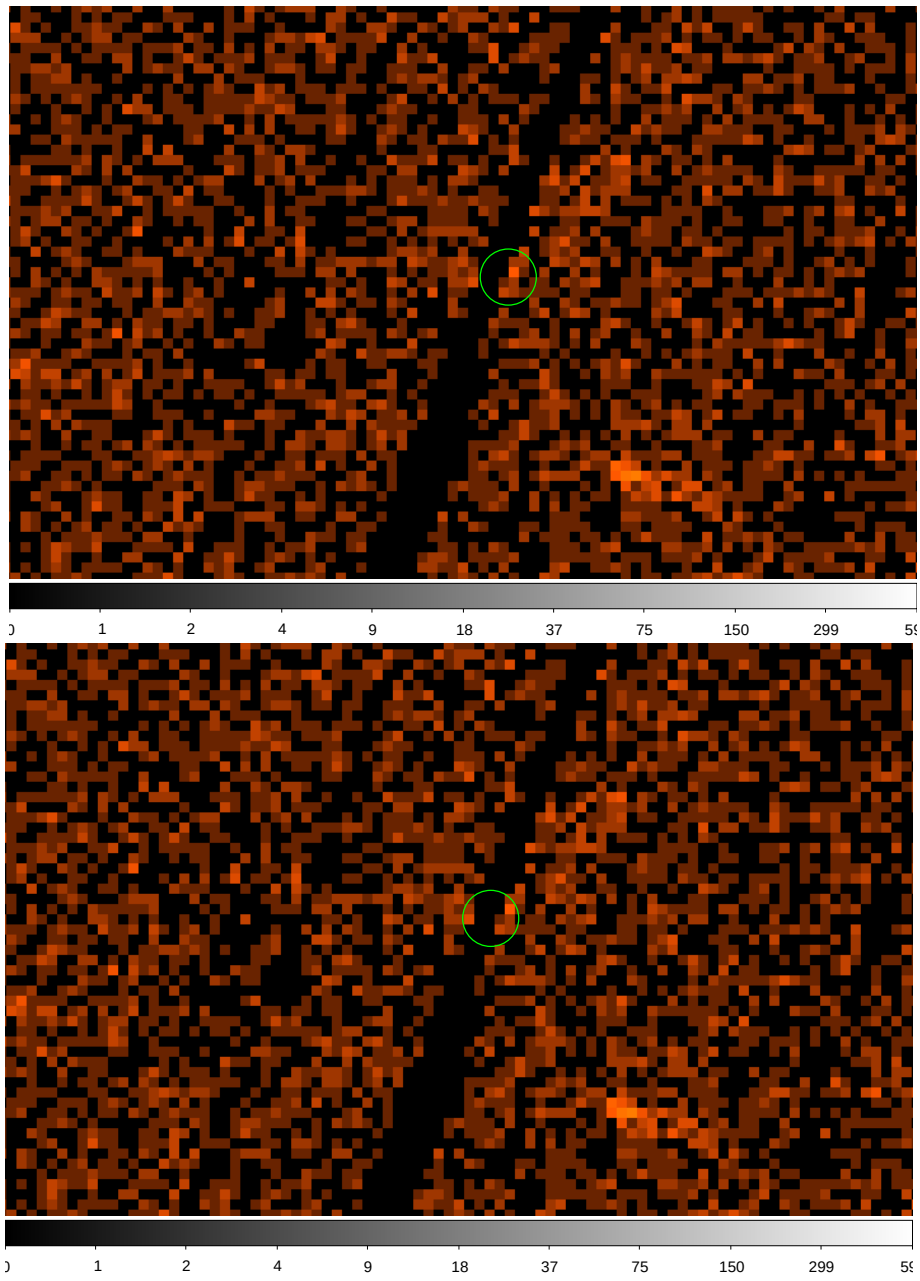

Figure 1: The effect of changing the boresight CCF on the positioning of a source circle, in detector coordinates, about a position RA: 359.6149, DEC: -60.8007 from observation 0760290601. Upper: with XMM_BORESIGHT_0024.CCF, Lower: with XMM_BORESIGHT_0026.CCF.

3.3 Time series correction

EPIC Light curves are corrected for instrumental effects by the task *epiclccorr* which uses *arfgen* to find the relative contribution of photons on each CCD to the total light curve. Once again, at the edge of the field of view, if close to a bad column or chip gap, important errors can be introduced by the conversion of sky to detector coordinates. In extreme cases this can cause the task to fail if an erroneous effective area of zero is returned. This problem will also be resolved by the new CCF.

4 Estimated Scientific Quality

The accuracy of conversions between the various celestial and detector-based coordinate systems, throughout the SAS, after this change is ~ 0.1 arcseconds. This remaining error is due to a combination of rounding errors and to real numbers (sky and detector pixels) being treated as integers in certain key routines within the code.

5 Test procedures and results

- Check for change in RA/DEC of sources

In principle the celestial position of sources returned by SAS should be unaltered by this change. We identified 28 observations (see table 2) spread evenly in time throughout the mission and chosen to have many point sources and no large regions of extended emission. The point source detection chain was run twice on these data with SAS v14 and the file XMM_BORESIGHT_0024.CCF and again with SAS v15 and XMM_BORESIGHT_0026.CCF, returning 6500 individual sources for EPIC-pn. In Fig. 2 we show the difference in source positions returned by these two runs for the EPIC-pn camera. The difference is negligible, with a standard deviation of the offset in RA and DEC of 5.8×10^{-3} and 6.5×10^{-3} arcseconds respectively. The small number of detections with a larger, up to 2 arcsecond, offset can be shown to be false detections caused by edge effects such as chip gaps or noise at the edge of a CCD. Figure 2 shows that the offsets are independent of distance from the optical axis. The exercise was repeated for the MOS cameras yielding a similarly negligible offset (see table 3).

- Check that OM and RGS are unaffected

The RGS and OM cameras should be completely unaffected by this change. To verify this, the wavelength of lines detected in the RGS cameras, for AB Dor (obsid: 01345214, 01551501, 01603628) and Capella (obsid: 05107802 and 05107811) were calculated separately with the BORESIGHT_0024 and 0026 CCFs. Differences were found to be negligible. The position of sources found in the OM source searching procedure for observations, 0402560201 (M31; 619 sources)and 0065820101 (NGC 1333; 51 sources) were also com-

Table 2: Observations used to check the offset error

Revolution	Obsid
102	0099020301
205	0100240201
304	0111240101
407	0065820101
528	0147511301
602	0143370101
735	0162160601
818	0202650101
905	0203360801
1016	0304320301
1104	0302310301
1201	0402560201
1363	0500500701
1419	0503560601
1530	0503240201
1633	0554540201
1712	0551150101
1805	0606030101
1941	0652450101
2018	0655860101
2103	0672780101
2235	0672960101
2312	0693520101
2410	0690500101
2534	0720750301
2618	0721400201
2736	0740040301
2821	0761920901

Table 3: Standard deviation of the celestial position offset between the old and new CCF

Camera	δRA	δDEC
	arcsec	arcsec
EPN	5.8×10^{-3}	6.5×10^{-3}
MOS-1	1.0×10^{-2}	4.0×10^{-2}
MOS-2	2.8×10^{-2}	2.5×10^{-2}

Table 4: Raw pixel coordinates of sources detected with the old and new CCFs

RA	DEC	Offax angle arcminutes	RAW (old) X/Y	RAW (new) X/Y	ecoordconv X/Y
EPIC-pn from observation 0065820101					
52.2386	31.2390	0.25	26/184	26/184	26.3/184.0
52.2299	31.2749	2.3	36/186	36/186	35.9/185.7
52.3929	31.2962	8.9	20/198	20/199	20.2/198.8
52.0457	31.2318	9.7	47/181	48/182	47.6/182.0
52.4468	31.6811	14.3	4/7	5/8	5.0/7.8
MOS-2 from observation 0655860101					
187.7087	1.2564	1.2	303/305	303/305	302.8/305.3
187.7547	1.3126	3.4	242/76	240/76	239.8/76.3
187.8269	1.2404	7.3	405/530	402/530	401.6/529.6
187.8767	1.2527	10.1	510/400	504/397	504.4/397.0
187.7071	1.0343	14.5	231/305	228/312	227.7/312.1

pared for the two boresight files and found to be identical to 4 decimal places.

- Check that raw pixel values for EPIC are now correct in source lists

The source detection task was run on the EPIC-pn observation 0065820101 (target: NGC 1333) with SAS v14 and XMM_BORESIGHT_0024.CCF and again with SAS v15 and XMM_BORESIGHT_0026.CCF. Source detection works on sky coordinate images and finds and returns celestial (RA, DEC) source positions. It then converts these back to the raw coordinates on the CCDs, going through the full chain of instrument-specific conversions, including reading and using the boresight CCF. The resulting, returned raw pixel positions of a number of sources at differing off-axis angles, were extracted and tabulated (Tab. 4). These were compared with the result of the conversion of celestial to RAW pixels made by the task *ecoordconv* using the 0026 boresight file. While the results are the same at small off-axis angles for the two CCFS, at larger off-axis angles only the values returned by this CCF release are correct. A similar comparison is provided for the MOS-2 camera and the observation 0655860101 (target: RX J1230.8+0115).

6 Compatibility

This CCF is only compatible with SAS version 15 and later. It has been given ALGOID=1 to avoid it being inadvertently used in earlier SAS versions. Similarly, SAS 15 will not use earlier versions of the Boresight CCF.

References

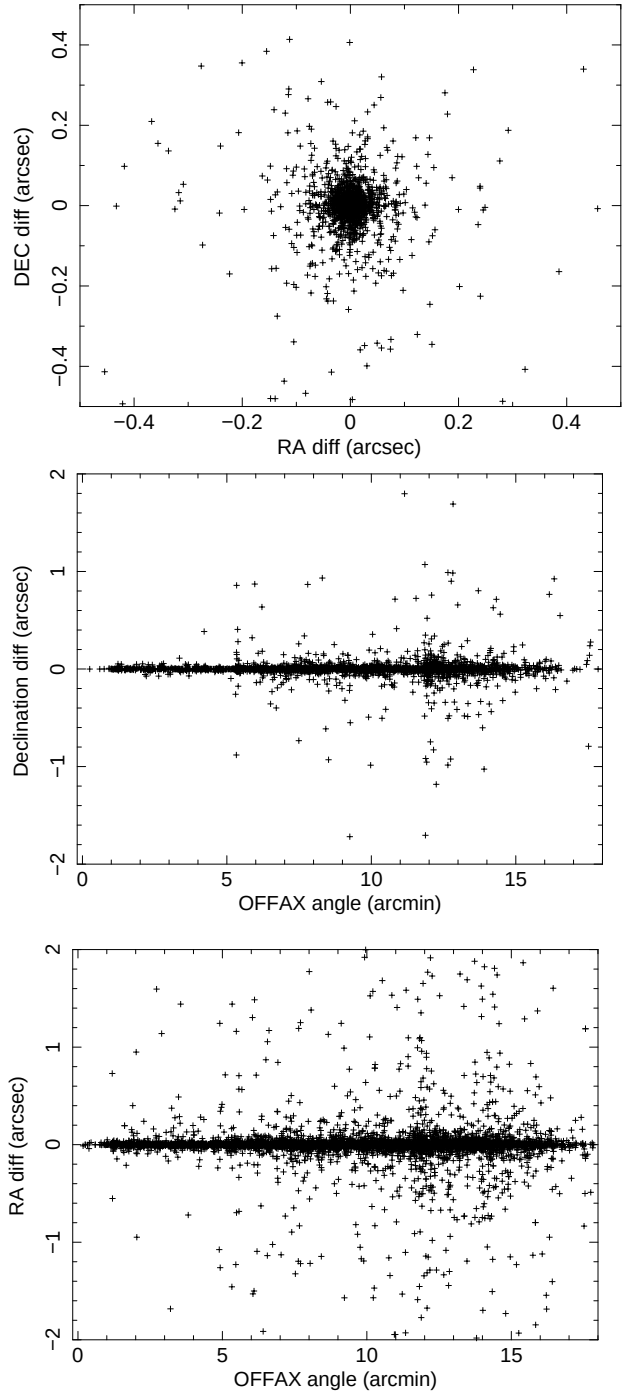

Figure 2: Differences between the celestial positions of EPIC-pn sources returned by SAS v14 with XMM_BORESIGHT_0024.CCF and SAS v15 with XMM_BORESIGHT_0026.CCF from a sample of 28 observations spread evenly in time from 2000 to 2015. Upper: Differences in RA and DEC of sources in the full sample; Middle: Difference in the declination of source positions as a function of the off-axis angle; Bottom: Difference in the right ascension of source positions as a function of the off-axis angle